Nanoscale

Hydrogen Bonded Trimesic Acid Networks on Cu(111) Reveal how Basic Chemical Properties are Imprinted in HR-AFM Images

Journal:	*Nanoscale*
Manuscript ID	NR-ART-07-2021-004471.R1
Article Type:	Paper
Date Submitted by the Author:	27-Aug-2021
Complete List of Authors:	Zahl, Percy; Brookhaven National Laboratory, CFN Yakutovich, Aliaksandr ; Ecole Polytechnique Federale de Lausanne, Laboratory of Molecular Simulation (LSMO), Institut des Sciences et Ingenierie Chimiques, Valais Ventura-Macias, Emiliano; Universidad Autonoma de Madrid, Departamento de Física Teórica de la Materia Condensada Carracedo-Cosme, Jaime; Universidad Autónoma de Madrid, Quasar Science Resources S.L., Camino de las Ceudas 2, E-28232, Las Rozas de Madrid, Spain and also Departamento de Física Teórica de la Materia Condensada Romero-Muñiz, Carlos; Universidad Autónoma de Madrid, Departamento de Física Teórica de la Materia Condensada Pou, Pablo; Universidad Autonoma de Madrid, Fisica Teorica de la Materia Condensada Sadowski, Jerzy; Brookhaven National Laboratory, Center Functional Nanomaterials Hybertsen, Mark; Brookhaven National Laboratory, Perez, Ruben; Universidad Autónoma de Madrid, Fisica Teorica de la Materia Condensada

SCHOLARONE™
Manuscripts

Hydrogen Bonded Trimesic Acid Networks on Cu(111) Reveal how Basic Chemical Properties are Imprinted in HR-AFM Images

Percy Zahl[*,1], Aliaksandr V. Yakutovich[2], Emiliano Ventura-Macías[3], Jaime Carracedo-Cosme[4], Carlos Romero-Muñiz[5], Pablo Pou[6], Jerzy T. Sadowski[1], Mark S. Hybertsen[1], Rubén Pérez[*,6]

[1] Center for Functional Nanomaterials, Brookhaven National Laboratory, Upton, NY 11973-5000, USA
E-mail: pzahl@bnl.gov
[2] Laboratory of Molecular Simulation (LSMO), Institut des Sciences et Ingenierie Chimiques, Valais, École Polytechnique Fédérale de Lausanne, CH-1951 Sion, Switzerland
[3] Departamento de Física Teórica de la Materia Condensada, Universidad Autónoma de Madrid, E-28049 Madrid, Spain
[4] Quasar Science Resources S.L., Camino de las Ceudas 2, E-28232 Las Rozas, Madrid, Spain and also Departamento de Física Teórica de la Materia Condensada, Universidad Autónoma de Madrid, E-28049 Madrid, Spain
[5] Departamento de Física Teórica de la Materia Condensada, Universidad Autónoma de Madrid, E-28049 Madrid, Spain and also Department of Physical, Chemical and Natural Systems, Universidad Pablo de Olavide, Ctra. Utrera Km. 1, E-41013, Seville, Spain
[6] Departamento de Física Teórica de la Materia Condensada, Universidad Autónoma de Madrid, E-28049 Madrid, Spain and also Condensed Matter Physics Center (IFIMAC), Universidad Autónoma de Madrid, E-28049 Madrid, Spain
E-mail: ruben.perez@uam.es
[*] Corresponding author

Abstract: *High resolution non-contact atomic force microscopy measurements characterize assemblies of trimesic acid molecules on Cu(111) and the link group interactions, providing the first fingerprints utilizing CO-based probes for this widely studied paradigm for hydrogen bond driven molecular self assembly. The enhanced submolecular resolution offered by this technique uniquely reveals key aspects of the competing interactions. Accurate comparison between full-density-based modeled images and experiment allows to identify key structural elements in the assembly in terms of the electron-withdrawing character of the carboxylic groups, interactions of those groups with Cu atoms in the surface, and the valence electron density in the intermolecular region of the hydrogen bonds. This study of trimesic acid assemblies on Cu(111) combining high resolution atomic force microscopy measurements with theory and simulation forges clear connections between fundamental chemical properties of molecules and key features imprinted in force images with submolecular resolution.*

Introduction

High resolution non-contact atomic force microscopy (HR-AFM) with functionalized metal tips terminated with closed-shell molecules like CO, or simply an oxygen atom, has revolutionized the field of molecular imaging. A CO attached to the apex of a metal tip provided a well-defined and inert tip termination that is able to reveal the internal structure of adsorbed organic molecules with unprecedented resolution [1, 2, 3, 4], identifying submolecular features either on metallic or insulating surfaces. [1, 3, 5] The imaging capabilities of HR-AFM with CO-metal tips were further extended to the determination of bond orders in aromatic compounds [6], the visualization of frontier orbitals [7] and the detailed study of features arising from the intermolecular interactions. [8, 9, 10] Moreover, this technique opened the door to track and control on-surface chemical reactions [11, 5, 12, 13, 14].

Self-assembled monolayers (SAM) of organic molecules are ordered assemblies spontaneously formed on surfaces upon adsorption. The self-organized state is achieved via weak intermolecular interactions between strong polar chemical groups, such as –OH, –NH_2, –COOH, –SH, etc [15]. The arrangement of the individual molecules and the stability of the remarkably large domains are controlled by the intermolecular forces and the molecule-substrate interactions. The structures formed by benzene-1,3,5-tricarboxylic acid (trimesic acid, TMA) present archetypical examples of SAM formation (see Fig. 1). The carboxylic acid groups lead to strong pairs of hy-

drogen bonds that are responsible for the self assembly. The resultant assemblies exhibit H-bonded networks that are characterized by a well-defined porous structure that can be obtained on a number of different substrates like graphite, [16, 17] Au(111), [18, 19, 20] Ag(111) [21] or Cu(111). [22] In the latter case, the TMA molecules are stabilized at 70 K into a hydrogen-bonded open cell network with a well defined set of possible orientations for the chemical structure of the basic SAM building block. A planar hexagonal arrangement is the most common TMA self-assembled structure with a pore size of ~ 10 Å. This porous structure has the ability of hosting an extra TMA molecule if the coverage increases [21, 23] and it can be used also for selective gas adsorption. [22]

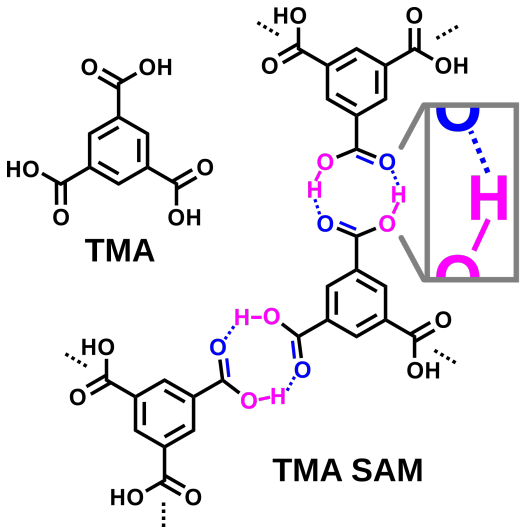

Figure 1: *1,3,5-Benzenetricarboxylic (Trimesic) Acid (TMA) and basic network junction building block of the H bonded (blue) SAM linked via the carboxylic groups.*

The application of HR-AFM with CO-decorated metal tips to the study of TMA SAMs on Cu(111) offers the possibility to gain new insight into the subtle changes induced in the bonding configurations and the electronic properties of the atoms involved in the hydrogen bonds. The small ordered domains formed at intermediate coverages allow us to compare the characteristics of carboxylic groups participating in hydrogen bonds with those that are not bonded by selecting molecules at the domain edge for imaging. Our methodology is based on a combination of high resolution HR-AFM in constant height mode for force imaging [1, 4] with first-principles calculations for both the atomic-scale characterization of the TMA adsorption and the formation of the SAM structure, and the theoretical simulation of the HR-AFM images.

The use of theoretical models has become essential to achieve a complete understanding of the HR-AFM experimental results, often difficult to rationalize otherwise. [24, 25, 26, 27] This point becomes particularly relevant when, due to a non-planar adsorption configuration, the variations in the charge density distribution and the electrostatic potential are significant along the tip-sample direction [27, 28, 24, 29]. In particular, the presence of carboxylic acids leads to specific features in the AFM images due to their charge distribution. [28, 30] To this end, we use our recently developed full-density-based method (FDBM) for the simulation of HR-AFM images [27]. This approach merges ideas presented in previous works [31, 32, 33, 26, 34] to describe the different force contributions to the HR-AFM images. It uses the tip and sample charge densities and the sample electrostatic potential obtained from density functional theory (DFT) calculations as input. Then just two fitting parameters are used to reproduce tip-sample forces retaining DFT accuracy, similarly to other purely first-principles methods [34, 35]. The resulting model is able to efficiently compute HR-AFM images, enabling extensive exploration of atomic scale structure and interpretation of the measured images.

Our study shows a rich and complex HR-AFM experimental contrast that is accurately reproduced by the theoretical simulations. This remarkable agreement makes a comprehensive characterization of the SAM structure at the atomic scale possible. More importantly, our results demonstrate how key features in the HR-AFM image directly arise from the chemical properties and environment (large model) of the molecule, providing thus a qualitative access to those features via the HR-AFM images. Our new results are complementary to recent studies demonstrating the impact of the wider environment of the molecule on the image [36, 37, 38]. In particular, we show how the electron withdrawing character of the carboxylic groups plays a crucial role in the HR-AFM contrast. The insight that basic chemical properties are strongly imprinted in the HR-AFM images may significantly contribute to the on-going efforts to achieve molecular identification based on HR-AFM images. [39]

Our results also contribute to the already long debate regarding the ability of HR-AFM to disclose H-bonds and other intermolecular interactions, as discussed in recent publications. [40, 8, 41, 42, 9, 43, 44, 10, 45, 46, 27]. Initially, it was pointed out that hydrogen bonds displayed subtle fingerprints in the HR-AFM images like thin lines or sharp boundary lines between areas of different brightness, [8, 40] and their physical origin was attributed to the charge redistribution resulting from the H-bond formation. [8, 10] Later, they were explained as an artifact due to the CO bending [43, 44]. Nowadays, there is an emerging consensus to attribute the intermolecular features to the spilling of the charge density of the molecules into the intermolecular region, [27, 42] an effect that is enhanced by the CO bending [32]. Our results on TMA support this point of view, ruling out that those features represent a true fingerprint of the H-bonds.

Results and Discussion

In this section we, first address the experimental growth of the TMA SAMs on Cu(111) and their characterization based on several techniques. We specifically use scanning tunneling microscopy (STM), low energy electron diffraction (LEED) and, especially, HR-AFM. Subsequently, we discuss the structure of the TMA SAMs at the atomic scale based on density functional (DFT) calculations and compare the theoretical HR-AFM images with the experimental results disclosing the main submolecular features. Lastly, we pay some attention to discuss the nature of the H-bonds in the TMA SAMs as well as their possible impact in HR-AFM imaging. Experimental and theoretical methods are described in the Supplemental Information.

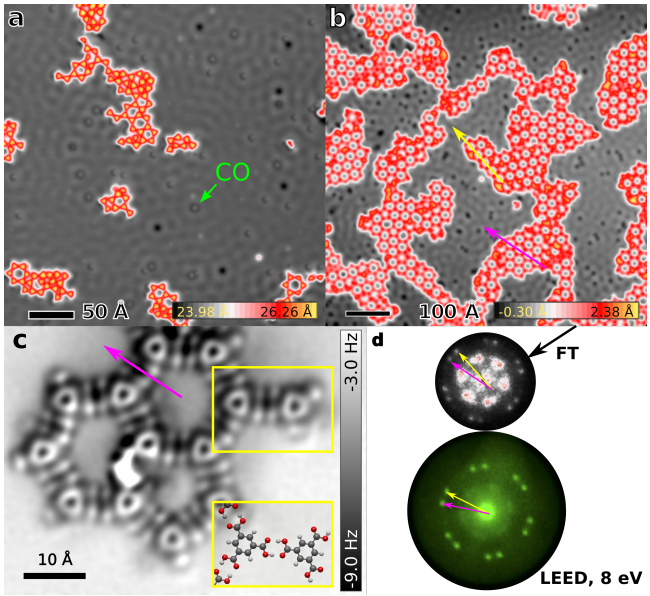

Figure 2: *(a) STM image of a medium TMA coverage with early double hydrogen bonded TMA network formation after annealing at 77 K with a small dose of CO added after cooling to 5K. The tiny bright spots with dark halo are CO molecules indicating a CO functionalized tip with a fairly symmetric coordinated CO molecule on the tip. (b) STM image of a higher coverage of a larger areas of double hydrogen bonded TMA networks after annealing for* 15 *min at* 70 *K. All STM images were acquired between* $80 - 100$ *mV and* $5 - 10$ *pA. (c) HR-AFM constant height image of the TMA network. Highlighted TMA dimer at the edge of the assembly. Structure Inset: Atomic dimer model with one possible hydrogen configuration. Imaging conditions were 100 mV bias for simultaneous current imaging at a height equivalent to a tunnel setpoint on Cu of 100 mV at 30 pA. (d) Top: Fourier transformed STM image of TMA network domains, Bottom: Comparison to LEED pattern. Scaled to match k-space dimensions.*

SAM Formation, Imaging and Large Scale Registry

We investigated the SAM formation by gradually increasing the TMA coverage from a very few individual molecules to a fully covered disordered scenario. The evolution of the coverage is shown in Fig. 2 and Fig. S1 of Supporting Information. To study the hydrogen bond formation, we focused on an intermediate coverage for which small TMA clusters formed on the surface as shown in Fig. 2a. Post deposition annealing of this surface at 70 K leads to the formation of a well-ordered, highly stabilized hydrogen-bonded, and mainly open-cell network as shown in the STM image in Fig. 2b. Figure 2c shows the power of HR-AFM imaging, exhibiting a detailed view of the TMA features when embedded in the SAM network. In particular, the submolecular structure of the TMA building blocks is resolved. Further HR-AFM images are shown in Sec. S1 of the Supporting Information. Now it is possible to assign the location of the individual TMA molecules.

The STM image in Fig. 2b, containing a large TMA network area, has been Fourier transformed as shown in Fig. 2d. For comparison, LEED experiments verify the formation of the TMA SAMs on Cu(111) and provide large area statistics on network registry. The comparison in Fig. 2d indicates that both measurements reveal the same basic features, in particular the six fold array of doubled spots in reciprocal space. Taken together, this data indicate that the film consists of 6 equivalent domains, rotated $30° \pm 6.2(0.5)°$ relative to the Cu[-110] direction and its equivalents, as illustrated for the LEED pattern shown in Fig. 3.

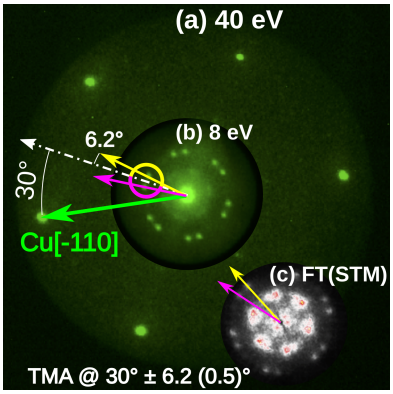

Figure 3: *TMA network registry identification via LEEM using LEED mode. (a,b) LEED at same scale and with low energy (*8 eV*) overlaid in the center. The TMA network cells (yellow/purple arrows, see corresponding arrows in STM Fig. 2b) are orientated relative to the Cu[-110] at* $30° \pm 6.2(0.5)°$ *as indicated. See also Fig. S8 for details.*

Multi-scale Model of the SAM on Cu (111)

The periodic structure, revealed by the LEED experiments, forms the basis for our multi-scale structural

study utilizing DFT calculations.

Our initial DFT calculations for individual TMA molecules on Cu(111) revealed that the adsorption of the monomer on the "hollow" site was ≈ 80 meV energetically more favorable compared to the "top" one. Here we refer to the position of the center of the benzene ring. Curiously, the situation changed for the TMA dimer. Two interacting molecules initially placed on "hollow" positions would cooperatively relax to adopt a "bridge" position instead (Fig. 4a.b). This happened because of the strong hydrogen bonds between two neighboring TMA molecules and the geometric misalignment of the TMA dimer with the underlying Cu(111) surface. At the same time the dimer placed initially on the "top"–"hollow" position would shift to a "top"–"bridge" position. However, the computed energy showed that the latter configuration was ≈ 100.0 meV less stable compared to the "bridge"-"bridge" one. These results are the key to understand the arrangement of TMA SAMs on Cu(111).

A six member ring can be formed with all of the TMA molecules placed on "bridge" sites. We refer to such a hexamer as "p". Indeed, our DFT simulations exploring ring assembly motifs showed that the "p" is the most stable hexamer configuration. However, due to the geometrical constraints in a periodic assembly, such a unit can only be surrounded by six neighboring hexamers that have four TMAs on top and two on bridge site. We refer to such hexamers as "q". According to our calculations the latter is higher in energy by ≈ 200 meV, as detailed in Sec. S2 of the Supporting Information. Combining "p" and "q" units one can reproduce the experimentally observed network, as shown in the Fig. 4d.

The atomic-scale details determined in our analysis of the TMA dimer, the basic structural motif of the SAM network, play a key role in the analysis of the HR-AFM images. The structure possesses two short hydrogen bonds of 1.54 Å (and 178° of OH$\cdots$O angle), consistent with typical bond lengths of strong H-bonds. [47] The averaged adsorption height is ~ 3.1 Å, typical of physisorbed molecules. However, there is a remarkable bending (0.71 Å) and tilting of the molecule due to the interaction with the substrate, as shown in Fig. 4b,c. In particular, the O atoms without H are pointing downwards to the substrate with an angle of up to $12°$. while OH$\cdots$O atoms have a weaker interaction with the substrate. The carboxylic groups participating in the hydrogen bonding remain planar. All tip–sample heights are referred to the average molecular plane (3.08 Å above the plane going through the center of the atoms in the top layer of the Cu substrate).

The strong interaction with the substrate competes with the hydrogen bonding. We calculated the strength of the H-bonds between two TMA molecules in gas phase. Since two H-bonds are formed, we normalize accordingly and find 440 meV per individual H-bond, in very good agreement with previous calculations [48, 23]. This is remarkably strong, well above the typical H-bond energy around ∼250 meV per bond [47]. For comparison, we calculated the dimer assembly energy between two adsorbed TMA molecules on Cu(111): $E_{\mathrm{dimer,ads}} - 2 \times E_{\mathrm{single,ads}}$. Here $E_{\mathrm{single,ads}} = E_{\mathrm{mol+Cu}} - E_{\mathrm{mol}} - E_{\mathrm{Cu}} =$ -1480 meV is the adsorption energy of a single TMA molecule on Cu(111), $E_{\mathrm{dimer,ads}} = E_{\mathrm{dimer+Cu}} - 2 \times E_{\mathrm{mol}} - E_{\mathrm{Cu}} =$ 3740 meV is the adsorption energy for the dimer, and E_{mol} and E_{Cu} are the total energy of the isolated molecule and the metal slab respectively. The result, 780 meV, leads to an effective, net binding value of 390 meV/bond. While this is approximately 11% smaller than in the gas phase, it clearly shows that the high strength of the hydrogen bonds is sufficient to overcome the interaction with the substrate of the two O atoms that have displaced downwards in the individually absorbed TMA molecules.

Analysis of the HR-AFM Images

A zoom in on the HR-AFM image of a dimer at the edge of the assembly is shown in Fig. 5a. There is a clear difference between the carboxyl groups that form hydrogen bonds, interior to the assembly and those at the edge of the assembly that do not form hydrogen bonds.

To understand the features in this image and the role of interaction with Cu(111) surface, we calculate the theoretical HR-AFM images of the molecules to compare with the experiments. The procedures are described in the methods section. We emphasize that the theoretical images presented are based on modeling the frequency shifts in strict parallel to the experimental imaging methodology. We have selected the most representative calculated images attending to the match with the experimental information and after a careful optimization of the parameters of the model. Other simulated images are shown in Sec. S3 of the Supporting Information.

The most appropriate tip-sample heights in our model are found to be between $z \sim 3.10$ Å and $z \sim 3.25$ Å, with $z = 3.17$ Å being the height showing the best match with experiments, as shown in Fig. 5b-d. Notice that these heights are referred to the average molecular plane (3.08 Å with respect to the substrate), so they correspond to absolute tip heights of ~ 6.18 Å, ~ 6.33 Å, and 6.25 Å above the Cu substrate.

The overall agreement between the theoretical calculations and the experiments is remarkable. Our HR-AFM calculations reproduce the main features of the experimental images. Specifically, we find: i) the triangular shape of the benzene rings rather than the expected hexagonal symmetry; ii) the clear difference in the appearance of the –COOH groups between those involved in the H-bonding, where the two oxygen atoms are clearly visible as long and bright branches, and those that are unbonded, with only one oxygen visible; and iii) the links of the oxygen atoms with the central ring, which appear as faint and not well defined lines

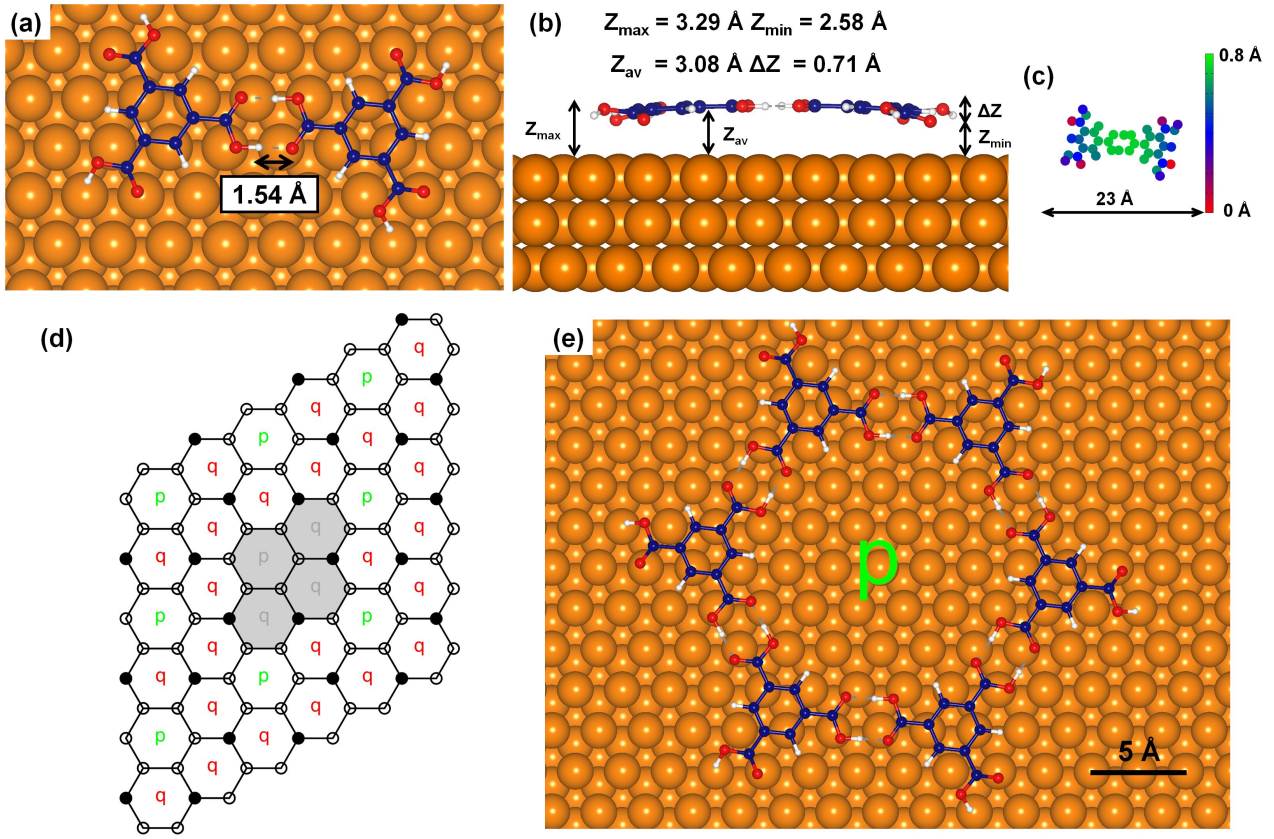

Figure 4: *Equilibrium structures of the TMA molecules adsorbed on Cu(111) represented with ball-and-stick models (C atoms blue. O atoms red and H atoms white). Top (a) and side (b) views of a TMA dimer chosen as the the minimal building block of the structure, displaying some relevant heights. Height distribution of the atoms of the molecule (c). Scheme of the large scale TMA "p-q" network cell model (d) as registered to the Cu(111) surface. The unit cell is highlighted in gray. The TMA molecules are represented by circles: empty ones for the on bridge location and filled ones for the on top location. One of typical pore structures of the long-range TMA network (e). See Sec. S2 of the Supporting information for more details.*

with suppression of the connecting carbon in the image. Similar characteristics have been observed for other molecules with carboxyl groups. [28, 30] The features of these images are directly related to the CO probe. In some cases, the influence of the metallic part of the tip is noticeable, [49, 50] but this is not the case in our TMA system as we discuss in Sec. S7 of the Supporting Information, explicitly checking that its contribution is negligible (see Fig. S18).

Notice that, in the H-bond areas, the theoretical images only display very thin lines surrounding an empty region. These faint lines are seen only for some tip-sample heights. Such thin lines are not observed in the experimental image. In addition, straight lines are seen connecting two oxygen atoms within each of these –COOH groups, where obviously there is no bond. Further, these features are much more pronounced than those very subtle lines in the H-bond area. These results conclusively support the emerging consensus about the significance of these intermolecular features observed in the HR-AFM images: they result from the tails of the charge density accumulated around the electronegative atoms which penetrate into the intermolecular region. This charge density affects the force at the typical range of heights above the molecule probed by the CO molecule [42, 27, 44]. This effect is completely unrelated to the charge redistribution associated with the H-bond formation, that takes place close to the molecular plane [27]. Thus, those lines are not a fingerprint of H-bonds as such [8, 10].

Interpretation of Chemical Features

The main message of our work is that the contrast in the HR-AFM images can be understood in terms of the chemical properties of the TMA molecules. More precisely, the key point to interpret the images relies on the electron withdrawing behavior of the COOH moieties.

Figure 6 shows the calculated HR-AFM image including the decomposed contributions provided by our model. In addition, we include two-dimensional profiles of the electron charge density and the electric field (z-component), the DFT inputs to the HR-AFM model. With this information, we are in a position to discuss in more depth the HR-AFM images. As we

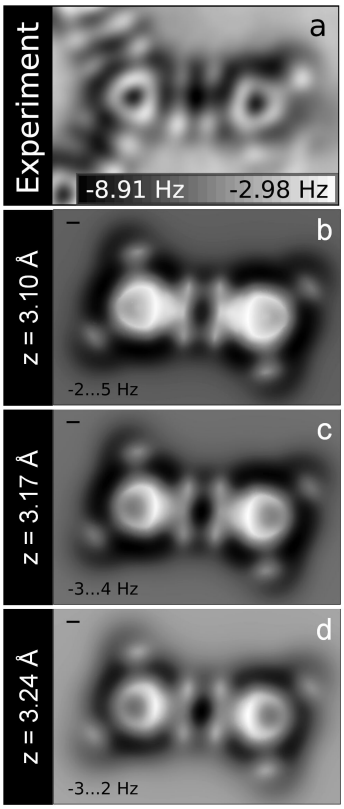

Figure 5: *Comparison between experiments and theory. Upper panel (a): zoom of the experimental HR-AFM image showing the detail of two H-bonded TMA molecules been only to the left part of a larger network (see Fig. 2). Three lower panels (b,c,d): We have selected three theoretical frequency shift maps of a TMA dimer at different tip-sample heights. The tip-sample heights, z, are considered from the averaged molecular plane, that is located 3.08 Å above the substrate. The length scale of the white/black bars in the theoretical images is 1 Å.*

have mentioned, the triangular shape of the molecule is a direct consequence of the symmetrical distribution of –COOH substituents. This circumstance leads to the well-defined triangular configuration of the electric field, that is responsible for a similar feature in the electrostatic contribution, giving rise to the final contrast displayed in the experimental and theoretical images. Notice that the charge density map (Fig. 6) shows a more hexagonal shape. At the relevant heights, the charge accumulates on the ring due to the larger spatial extension of aromatic π orbitals. This charge density distribution, through the short-range Pauli repulsion and the induced probe relaxation, would lead to the typical hexagonal image, where the bright lines associated to the C–C bonds correspond to the saddle lines of this purely repulsive potential energy surface (PES). However, The inclusion of the electrostatic field in the PES probed by the CO tip leads to a net shift of the saddle lines towards less electrostatically attractive areas, where the total interaction is more repulsive, resulting in the final triangular shape observed in the images. [51, 28]

The triangular shape is just one of the striking features in the HR-AFM images associated with the strong electron withdrawal character of the the COOH groups. The HR-AFM fingerprint of the COOH groups can be also understood in terms of the electron charge redistribution among the atoms in these groups. If we analyze the charge density, we can appreciate how the charge spreads onto the O atoms, leaving the central C atom with a lower charge density. The repulsive short-range interaction, that senses this charge accumulation, made the O atoms visible. Moreover, the electric field around the oxygen atoms is repulsive, due to their lone pairs, and further contributes to clearly resolve the O atoms in the HR-AFM images, as seen in the total force static map in Fig. 6. More importantly, the electric field produces a modification of the PES that is reflected in the long ovals or lines extending through these areas when the probe relaxation is taken into account (panel Total(relaxed) in Fig. 6). The same electronic distribution is responsible for the fact that the central C atoms of the COOH groups are not resolved, leading to images with faint lines linking directly the outer oxygen atoms with the central benzene ring.

Notice that the AFM fingerprint of carboxylic groups is different between those groups involved in H-bonded links to a neighboring carboxylic group and those that are not so linked. Free (not H-bonded) COOH groups only show one bright spot, corresponding to the OH termination; this is due to the surface induced distortion of the -O termination (see Fig. S11 for more profiles at other tip heights). The absence of the H-bond favors the interaction with the metal substrate promoting the bending of the O atoms downwards. However, in the presence of a neighboring molecule, the strength of the H-bond prevails and prevents this downshift. The general tilting of the molecule can be also discerned in the HR-AFM images. In order to evaluate the influence of possible adsorption changes in the described AFM features of TMA molecules, we have explored other stable configurations of the TMA molecules (see Fig. S15). Basically, we can observe how changes in the height distribution induced by the different adsorption configurations on the substrate produce only minor variations in the AFM images (higher atoms produce simply brighter AFM features), but no dramatic changes in the main features are observed.

Additionally, the dehydrogenation of a non H-bonded -COOH groups has been observed on molecules with carboxylic acids adsorbed on metallic surfaces. [30] It seems that this effect is not happening in our molecules as revealed by our AFM analysis. Such a dehydrogenation (carboxylic to carboxylate) would strongly modify the molecular configuration, shifting down that the corresponding COO-group and also a part of the molecule which would lead to a significantly different AFM image (see Fig. S16).

Another important point that deserves some attention is the presence of nuclear quantum effects, as pro-

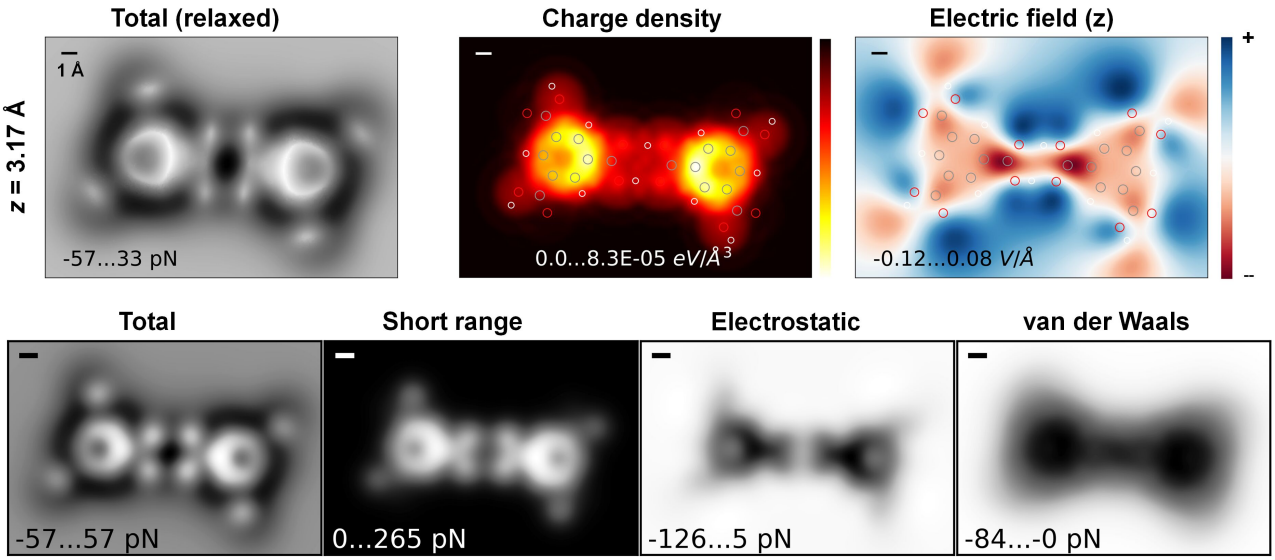

Figure 6: *Theoretical force maps of the TMA dimer together with the two-dimensional profiles of electron charge density and the z-component of the electric field at $z = 3.17$ Å. The decomposed contributions of the unrelaxed force maps at the same height: Short range, electrostatic and van der Waals components (lower panel). In this context, unrelaxed means that we have not included the tilting contribution of the model. See Sec. S3 in the Supporting Information.*

ton tunnelling or zero-point motion, that may appear on H-bonded systems. On carboxylic acids forming the two parallel H-bonds, there are two similar configurations depending on the protons position either in the two opposite corners of the rectangle shaped by the four oxygen atoms involved in the two H-bonds, or in the other two corners (see Sec. S6 in the Supporting Information for further details). As stated by the resonance-assisted hydrogen bonding model, [52, 53] the presence of proton tunnelling could induce a quantum resonance state between the two configurations, enhancing the strength of the H bonds. This state is characterized by placing, in average, the protons at the middle of the bonds.

We analyzed the potential energy surface controlling this proton motion, as described in the Supporting Information. Our calculations for the TMA dimer on the Cu(111) show an energy barrier between the two stable configurations of 122 meV (see middle panel of Fig. S17). Thus, in principle, a similar proton tunnelling could be expected. Therefore, the hydrogen atoms could be: (i) at two oxygen atoms placed on opposite corners, (ii) in the other two oxygen atoms, or (iii) at the middle of the H-bonds.

The question that arises is: could the HR-AFM disclose the position of these hydrogen atoms? The very small charge density associated with the hydrogen atoms makes them invisible to the probe (see Fig. S17). However, as recently shown for tautomerization of meso-Dibenzoporphycene molecules on different substrates [54] or for concerted proton movement on chains of 2,5-diamino-1,4-benzoquinonediimines, [55] when hydrogen movement induces significant changes in the absorption configuration, HR-AFM images can be used to determine, indirectly, its position. In our TMA system, although our simulated HR-AFM images do barely distinguish three possibilities (see lower panel of Fig. S17), experimental resolution together with other factors, (e.g. defects and molecular strain), prevent the observation of these subtle features related to the H location. Thus, for this particular system we cannot conclusively determine the proton position at the H-bonds, and therefore, we can neither prove nor discard any fingerprint of proton tunnelling.

In order to determine the proton position the combination of HR-AFM with other techniques could provide a more direct and reliable access to the local distribution of the electric field created by the molecule [51, 56, 57] rather than the mere inspection of HR-AFM images. In particular, the powerful combination of HR-AFM, STM and tip-enhanced Raman scattering (TERS) recently released by Xu et al. [58] seems to be the most promising experimental set up to tackle this problem.

Conclusions

Assemblies of TMA on diverse surfaces driven by strong pairs of hydrogen bonds have been widely studied. In the first measurements that exploited the high resolution of HR-AFM with CO functionalized tips for this prototypical molecular self assembly, we have investigated the interplay between the carboxylic group interactions with the Cu(111) substrate and with each other. We specifically focused on small-scale assemblies with the commonly observed porous, hexagonal network so that carboxylic groups at the edge of the assembly can be directly compared to those forming hydrogen bonds in the interior of the assembly. The HR-

AFM images revealed clear and distinct fingerprints for these two types of interaction. Furthermore, the strong attraction of electronic charge from the π-system by the COOH groups led to a significant distortion of the central carbon ring in the HR-AFM images of the TMA molecules.

We used first principles calculations based on DFT to determine low energy configurations for the adsorbed TMA molecules on Cu(111) and the formation of hydrogen bonded dimers and hexamers. The calculations demonstrated the structural distortions of the molecule driven by strong interactions between the lone O atom on the carboxylic group and surface Cu atoms. Considering a TMA dimer on the surface, the registry of the TMA molecules on the Cu(111) shifted to accommodate both the formation of the dual hydrogen bonds between the TMA molecules and the remaining interactions with the Cu surface atoms. At the next level of assembly, a basic six-fold ring of TMA could be assembled out of optimized dimers. However, a more extended network could only be formed by alternating optimal and shifted six-fold rings of TMA, resulting in an overall assembly whose structure agreed with both the HR-AFM and LEED experiments.

A key element of this study was closing the loop between the energy-minimized molecular structural motifs identified in the DFT-based calculations and the HR-AFM observations. We used the recently developed full-density-based method to simulate the HR-AFM images based on inputs from the DFT calculations. The excellent agreement between the simulated and measured images validated the underlying, atomic-scale motifs that had been identified and supported a clear physical interpretation of the fingerprints observed in the measurements.

Our results for the prototypical case of TMA assembly on Cu(111) illustrate the power of combining the intramolecular resolution of the HR-AFM and an accurate first-principles based approach to simulate the images. By thus connecting atomic scale models directly to the experiments, the expression of fundamental chemical features in the molecules in the measured images can be understood. In particular, we have shown how the strong electron withdrawing character of the COOH groups leads to the electrostatic contribution to the total force that controls the nontrivial sub-molecular contrast of the HR-AFM images. These striking features include the molecules appearing with triangular inner rings, instead of the expected hexagons, and the suppression of the central C atoms in the COOH groups. This asymmetric contrast in HR-AFM images is not a consequence of the lack of aromaticiy but instead it appears in the image due to the electrostatic potential of the molecule. These links among basic properties of chemical groups, their contribution to the tip-sample interaction and the contrast of HR-AFM images represent a significant step in the on-going quest to develop tools that enable chemical interpretation of scanning probe images.

Finally, we have paid special attention to the description of H-bonds in the HR-AFM experiments, without finding any definitive fingerprints. In the experimental images no evidence for the direct visualization of H-bonds is found while theoretical calculations display very faint intermolecular features, less marked than lines joining oxygens in the same COOH group, for some tip heights. However, these features are a consequence of the charge density of the electronegative atoms of the molecules rather than a real HR-AFM fingerprint of the intermolecular interactions.

Acknowledgements

This research used resources of the Center for Functional Nanomaterials (CFN), which is the U.S. DOE Office of Science User Facility, at Brookhaven National Laboratory under Contract No. DE-SC0012704. In particular, the LT-STM/HR-AFM facility at CFN was used for all experiments and imaging and resources at the Scientific Data and Computing Center of the Computational Science Initiative was used for computations at the CFN. Special thanks to Fernando Camino from CFN for support using the FIB for Q-Plus sensor tip preparations. E. V.-M., J. C.-C., C. R.-M., P. P. And R. P. acknowledge the financial support from the Spanish MINECO (AEI/FEDER, UE project MAT2017-83273-R), from the Comunidad de Madrid (project IND2017/IND-7793) in collaboration with Quasar Scientific Resources SL, and from the Spanish Ministerio de Ciencia e Innovación, through the "María de Maeztu" Programme for Units of Excellence in R&D (grant No. CEX2018-000805-M). The Swiss National Supercomputing Center (CSCS) and the Red Española de Supercomputación (RES) at the Marenostrum Supercomputer (BSC, Barcelona) are acknowledged for providing computational resources. We thank Prokop Hapala for initial runs of AFM simulations and discussions.

Supporting Information:

S1 Extra STM/HR-AFM images; S2 Structural analysis of the TMA SAM; S3 Further results of the theoretical HR-AFM images; S4 Simulated AFM images of other TMA configurations; S5 Dehydrogenated form of TMA molecule; S6 Proton tunneling exchange; S7 Influence of the metal apex on HR-AFM images; S8 Experimental and computational methods

Author contributions:

PZ performed the experiments and the LEED data analysis, derived the initial structural model (including "P-Q") for AFM simulations and DFT calculations, and coordinated the whole project. JTS provided the experimental LEEM/LEED data. AVY performed DFT calculations (CP2K). MSH performed preliminary DFT

calculations (VASP). EVM and JCC performed HR-AFM simulations. CRM performed DFT calculations (VASP) PP and RP supervised DFT calculations and HR-AFM simulations. PZ, JTS, AVY, MSH, CRM, PP, RP wrote the paper. All authors discussed the results and the manuscript.

Abbrevations:

STM (Scanning Tunneling Microscopy); HR-AFM (High Resolution (Non-Contact) Atomic Force Microscopy); LEED (Low Energy Electron Diffraction); LEEM (Low Energy Electron Microscopy); FIB (Focused Ion Beam); SAM (Self-Assambled Monolayer); TMA (Trimesic Acid); DFT (Density Functional Theory); PES (Potential Energy Surface); FDBM (Full-Density-Based Method); CI-NEB (Climbing Image Nudged Elastic Band).

References

[1] L. Gross, F. Mohn, N. Moll, P. Liljeroth, G. Meyer, *Science* **2009**, *325*, 1110.

[2] L. Gross, F. Mohn, P. Liljeroth, J. Repp, F. J. Giessibl, G. Meyer, *Science* **2009**, *324*, 1428–1431.

[3] L. Gross, F. Mohn, N. Moll, G. Meyer, R. Ebel, W. M. Abdel-Mageed, M. Jaspars, *Nat. Chem.* **2010**, *2*, 821.

[4] L. Gross, *Nat. Chem.* **2011**, *3*, 273–279.

[5] A. Riss, S. Wickenburg, P. Gorman, L. Z. Tan, H.-Z. Tsai, D. G. de Oteyza, Y.-C. Chen, A. J. Bradley, M. M. Ugeda, G. Etkin, S. G. Louie, F. R. Fischer, M. F. Crommie, *Nano Lett.* **2014**, *14*, 2251–2255.

[6] L. Gross, F. Mohn, N. Moll, B. Schuler, A. Criado, E. Guitián, D. Peña, A. Gourdon, G. Meyer, *Science* **2012**, *337*, 1326–1329.

[7] L. Gross, N. Moll, F. Mohn, A. Curioni, G. Meyer, F. Hanke, M. Persson, *Phys. Rev. Lett.* **2011**, *107*, 086101.

[8] J. Zhang, P. Chen, B. Yuan, W. Ji, Z. Cheng, X. Qiu, *Science* **2013**, *342*, 611–614.

[9] S. Kawai, T. Nishiuchi, T. Kodama, P. Spijker, R. Pawlak, T. Meier, J. Tracey, T. Kubo, E. Meyer, A. S. Foster, *Sci. Adv.* **2017**, *3*, e1603258.

[10] H. Mönig, S. Amirjalayer, A. Timmer, Z. Hu, L. Liu, O. Díaz Arado, M. Cnudde, C. A. Strassert, W. Ji, M. Rohlfing, H. Fuchs, *Nat. Nanotech.* **2018**, *13*, 371–375.

[11] D. G. de Oteyza, P. Gorman, Y.-C. Chen, S. Wickenburg, A. Riss, D. J. Mowbray, G. Etkin, Z. Pedramrazi, H.-Z. Tsai, A. Rubio, M. F. Crommie, F. R. Fischer, *Science* **2013**, *340*, 1434–1437.

[12] A. Riss, A. P. Paz, S. Wickenburg, H.-Z. Tsai, D. G. De Oteyza, A. J. Bradley, M. M. Ugeda, P. Gorman, H. S. Jung, M. F. Crommie, A. Rubio, F. R. Fischer, *Nat. Chem.* **2016**, *8*, 678.

[13] N. Kocić, X. Liu, S. Chen, S. Decurtins, O. Krejcí, P. Jelínek, J. Repp, S.-X. Liu, *J. Am. Chem. Soc.* **2016**, *138*, 5585–5593.

[14] S. Zint, D. Ebeling, T. Schlöder, S. Ahles, D. Mollenhauer, H. A. Wegner, A. Schirmeisen, *ACS Nano* **2017**, *11*, 4183–4190.

[15] S. M. Barlow, R. Raval, *Surf. Sci. Rep.* **2003**, *50*, 201–341.

[16] S. Griessl, M. Lackinger, M. Edelwirth, M. Hietschold, W. M. Heckl, *Single Mol.* **2002**, *3*, 25–31.

[17] M. Lackinger, S. Griessl, W. M. Heckl, M. Hietschold, G. W. Flynn, *Langmuir* **2005**, *21*, 4984–4988.

[18] Y. Ye, W. Sun, Y. Wang, X. Shao, X. Xu, F. Cheng, J. Li, K. Wu, *J. Phys. Chem. C* **2007**, *111*, 10138–10141.

[19] H. Liang, W. Sun, X. Jin, H. Li, J. Li, X. Hu, B. K. Teo, K. Wu, *Angew. Chem. Int. Ed.* **2011**, *50*, 7562–7566.

[20] V. Iancu, K.-F. Braun, K. Schouteden, C. Van Haesendonck, *Langmuir* **2013**, *29*, 11593–11599.

[21] M. S. Baviloliaei, L. Diekhöner, *Phys. Chem. Chem. Phys.* **2014**, *16*, 11265–11269.

[22] N. Lin, D. Payer, A. Dmitriev, T. Strunskus, C. Wöll, J. V. Barth, K. Kern, *Angew. Chem. Int. Ed.* **2005**, *44*, 1488–1491.

[23] A. Ibenskas, M. Šimėnas, K. J. Kizlaitis, E. E. Tornau, *J. Phys. Chem. C* **2019**, *123*, 3552–3559.

[24] P. Jelínek, *J. Phys.: Condens. Matter* **2017**, *29*, 343002.

[25] J. R. Chelikowsky, D. Fan, A. J. Lee, Y. Sakai, *Phys. Rev. Mater.* **2019**, *3*, 110302.

[26] M. Ellner, N. Pavliček, P. Pou, B. Schuler, N. Moll, G. Meyer, L. Gross, R. Peréz, *Nano Lett.* **2016**, *16*, 1974–1980.

[27] M. Ellner, P. Pou, R. Pérez, *ACS Nano* **2019**, *13*, 786–795.

[28] J. van der Lit, F. Di Cicco, P. Hapala, P. Jelinek, I. Swart, *Phys. Rev. Lett.* **2016**, *116*, 096102.

[29] J. Peng, J. Guo, P. Hapala, D. Cao, R. Ma, B. Cheng, L. Xu, M. Ondrácek, P. Jelínek, E. Wang, Y. Jiang, *Nat. Commun.* **2018**, *9*, 122.

[30] P. Procházka, M. A. Gosalvez, L. Kormoš, B. de la Torre, A. Gallardo, J. Alberdi-Rodriguez, T. Chutora, A. O. Makoveev, A. Shahsavar, A. Arnau, P. Jelínek, J. Čechal, *ACS Nano* **2020**, *14*, 7269–7279.

[31] N. Moll, L. Gross, F. Mohn, A. Curioni, G. Meyer, *New J. Phys.* **2012**, *14*, 083023.

[32] P. Hapala, G. Kichin, C. Wagner, F. S. Tautz, R. Temirov, P. Jelínek, *Phys. Rev. B* **2014**, *90*, 085421.

[33] P. Hapala, R. Temirov, F. S. Tautz, P. Jelínek, *Phys. Rev. Lett.* **2014**, *113*, 226101.

[34] Y. Sakai, A. J. Lee, J. R. Chelikowsky, *Nano Lett.* **2016**, *16*, 3242–3246.

[35] D. Fan, Y. Sakai, J. R. Chelikowsky, *Nano Lett.* **2019**, *19*, 5562–5567.

[36] Z. Yang, C. Lotze, M. Corso, S. Baum, K. J. Franke, J. I. Pascual, *Small* **2019**, *15*, 1804713.

[37] L. L. Patera, X. Liu, N. Mosso, S. Decurtins, S.-X. Liu, J. Repp, *Angew. Chem. Int. Ed.* **2017**, *56*, 10786–10790.

[38] R. Ma, D. Cao, C. Zhu, Y. Tian, J. Peng, J. Guo, J. Chen, X.-Z. Li, J. S. Francisco, X. C. Zeng, L.-M. Xu, E.-G. Wang, Y. Jiang, *Nature* **2020**, *577*, 60–63.

[39] B. Alldritt, P. Hapala, N. Oinonen, F. Urtev, O. Krejci, F. Federici Canova, J. Kannala, F. Schulz, P. Liljeroth, A. S. Foster, *Sci. Adv.* **2020**, *6*, eaay6913.

[40] C. Weiss, C. Wagner, R. Temirov, F. S. Tautz, *J. Am. Chem. Soc.* **2010**, *132*, 11864–11865.

[41] A. M. Sweetman, S. P. Jarvis, H. Sang, I. Lekkas, P. Rahe, Y. Wang, J. Wang, N. R. Champness, L. Kantorovich, P. Moriarty, *Nat. Commun.* **2014**, *5*, 3931.

[42] A. J. Lee, Y. Sakai, M. Kim, J. R. Chelikowsky, *Appl. Phys. Lett.* **2016**, *108*, 193102.

[43] N. Pavliček, B. Fleury, M. Neu, J. Niedenführ, C. Herranz-Lancho, M. Ruben, J. Repp, *Phys. Rev. Lett.* **2012**, *108*, 086101.

[44] S. K. Hämäläinen, N. van der Heijden, J. van der Lit, S. den Hartog, P. Liljeroth, I. Swart, *Phys. Rev. Lett.* **2014**, *113*, 186102.

[45] A. Shiotari, Y. Sugimoto, *Nat. Commun.* **2017**, *8*, 14313.

[46] M. Ellner, P. Pou, R. Pérez, *Phys. Rev. B* **2017**, *96*, 075418.

[47] S. Scheiner, *Hydrogen Bonding: A Theoretical Perspective*, Oxford University Press, **1997**.

[48] J. M. MacLeod, Z. Ben Chaouch, D. F. Perepichka, F. Rosei, *Langmuir* **2013**, *29*, 7318–7324.

[49] D. Z. Gao, J. Grenz, M. B. Watkins, F. Federici Canova, A. Schwarz, R. Wiesendanger, A. L. Shluger, *ACS Nano* **2014**, *8*, 5339–5351.

[50] F. Schulz, J. Ritala, O. Krejčí, A. P. Seitsonen, A. S. Foster, P. Liljeroth, *ACS Nano* **2018**, *12*, 5274–5283.

[51] P. Hapala, M. Švec, O. Stetsovych, N. J. van der Heijden, M. Ondrácek, J. van der Lit, P. Mutombo, I. Swart, P. Jelínek, *Nat. Commun.* **2016**, *7*, 11560.

[52] G. Gilli, P. Gilli, *J. Mol. Struct.* **2000**, *552*, 1–15.

[53] L. Sobczyk, S. J. Grabowski, T. M. Krygowski, *Chem. Rev.* **2005**, *105*, 3513–3560.

[54] T. K. Shimizu, C. Romero-Muñiz, O. Stetsovych, J. Carracedo-Cosme, M. Ellner, P. Pou, K. Oohora, T. Hayashi, R. Perez, O. Custance, *J. Phys. Chem. C* **2020**, *124*, 26759–26768.

[55] A. Cahlík, J. Hellerstedt, J. I. Mendieta-Moreno, M. Švec, V. M. Santhini, S. Pascal, D. Soler-Polo, S. I. Erlingsson, K. Výborný, P. Mutombo, O. Marsalek, O. Siri, P. Jelínek, *ACS Nano* **2021**, *15*, 10357–10365.

[56] L. Gross, N. Moll, F. Mohn, G. Meyer, *Nature Nanotech* **2012**, *7*, 227–231.

[57] S. Fatayer, F. Albrecht, Y. Zhang, D. Urbonas, D. Peña, N. Moll, L. Gross, *Science* **2019**, *365*, 142–145.

[58] J. Xu, X. Zhu, S. Tan, Y. Zhang, B. Li, Y. Tian, H. Shan, X. Cui, A. Zhao, Z. Dong, J. Yang, Y. Luo, B. Wang, J. G. Hou, *Science* **2021**, *371*, 818–822.